Catalysis Today 148 (2009) 148–152

Contents lists available at ScienceDirect

Catalysis Today

journal homepage: www.elsevier.com/locate/cattod

# Hollow mesoporous silica sphere supported cobalt catalysts for F–T synthesis

Junhua Li [a,b], Yao Xu [a,*], Dong Wu [a], Yuhan Sun [a,*]

[a] State Key Laboratory of Coal conversion, Institute of Coal Chemistry, Chinese Academy of Sciences, Taiyuan 030001, China
[b] Graduate University of the Chinese Academy of Sciences, Beijing 10049, China

ARTICLE INFO

*Article history:*
Available online 23 April 2009

*Keywords:*
Fischer–Tropsch synthesis
HMSS
Cobalt
Catalyst

ABSTRACT

High dispersion $Co_3O_4$ nano-particles supported on hollow mesoporous silica spheres (HMSS) with bimodal pore distribution were prepared by "two-solvent" technique. As-synthesized catalysts were characterized by XRD, $N_2$ adsorption–desorption, XPS, SEM, TEM, and $H_2$-TPR. The results showed that $Co_3O_4$ nano-particles were present inside the pore system of HMSS and the particles sizes increased with the increasing loaded cobalt content. The catalysts show good performance and high selectivity of $C_5$–$C_{18}$ hydrocarbon in F–T synthesis, which should attribute to the unique bimodal pore distribution facilitating reactants to access the active sites and to transport higher hydrocarbon products.



## 1. Introduction

Cobalt catalysts for CO hydrogenation are the excellent ones to convert coal and natural gas to clean, environmental-sounded fuels and chemicals via syngas [1], because of their high Fischer–Tropsch (F–T) activity, selectivity for linear hydrocarbons and low activity for water-gas shift reaction (WGS). Supported cobalt catalysts [2–4] have been found to be promising catalysts for F–T synthesis. In order to gain high metal dispersion, cobalt is typically supported on oxides with high surface area, such as silica [5,6], alumina [2,7,8], titania [9,10] and zeolites [11,12]. The texture and chemical properties of support have important influence on the activity and product selectivity of Co catalysts [13,14].

Recently, well-defined mesoporous molecular sieves have been used as the support to prepare cobalt catalysts. There include MCM-48 [5], MCM-41 [15], SBA-15 [16], and HMS [17]. Manuel Arruebo et al. [18] used a wet impregnation technique to deposit $Fe_2O_3$ on hollow mesoporous silica spheres (HMSS). $Fe_2O_3$ clusters with a uniform size were present at the external surface of HMSS. Small-size clusters could also be seen in the mesoporous channels and the interior void space of HMSS. Because of the hollow structure of HMSS, the interior cavities could offer more location to deposit catalyst and provide better transport channels for reactants to access the active centers and for products to move out. Lopes et al. [19] deposited cobalt nano-particles inside the pores of SBA-15 using the "two-solvent" technique. This method is based on a volume of aqueous solution equal to the pore volume of the silica support (determined by $N_2$ sorption). The interest of this technique lies in loading cobalt species in the pores of support and minimizing the crystallization of $Co_3O_4$ particles on the external surface of the silica grains. However, the application of HMSS as the supports for cobalt catalyst prepared by using "two-solvent" technique is not reported so far.

In this work, hollow mesoporous silica spheres (HMSS) were used as a support of cobalt catalyst for Fischer–Tropsch synthesis. High dispersion $Co_3O_4$ nano-particles supported on HMSS were prepared by "two-solvent" technique. The catalysts showed good activity and high selectivity $C_{5+}$ hydrocarbons in F–T synthesis.

## 2. Experimental

### 2.1. Synthesis of catalysts

HMSS were prepared following references [20]. In a typical synthesis, a total of 39.2 g of hexadecyltrimethylammonium bromide (CTAB) followed by 46 g $Na_2SiO_3{\cdot}9H_2O$ were dissolved in 674 ml of water, resulting in a clear solution. Afterwards 70 ml ethyl acetate was quickly added, the mixture was homogenized and the stirring was stopped. The resulted mixture was allowed to stand at 303 K for 5 h, and finally aged at 90 °C for 48 h. the solid product was collected by filtration, washed several times with deionized water and ethanol, and dried overnight at 323 K. The template was removed by calcination at 823 K for 20 h in flowing air.

Cobalt catalyst was prepared by dispersing calcined HMSS powders in dry *n*-hexane. After stirring for 30 min, a small amount of water (second solvent, its volume was equal to the pore volume of the HMSS, determined by $N_2$ sorption, typically 2 $cm^3/g$ of silica) with determinated amount of $Co(NO_3)_3$ was added dropwise into the suspension. The mixture was stirred for 48 h, filtrated, dried at

* Corresponding author. Tel.: +86 351 4049859 fax: +86 351 4041153.
*E-mail addresses:* xuyao@sxicc.ac.cn (Y. Xu), yhsun@sxicc.ac.cn (Y. Sun).

0920-5861/$ – see front matter © 2009 Elsevier B.V. All rights reserved.
doi:10.1016/j.cattod.2009.02.046

363 K for 5 h, and calcined at 673 K for 4 h. The resultant catalyst was designated as *TX*, where *X* represented the cobalt mass content. A regular catalyst MCM-41(30) supported on MCM-41 was prepared in the same method (cobalt mass content 30%).

### 2.2. Characterization

$N_2$ adsorption/desorption isotherms at 77 K were measured using a Micromeritics Tristar 3000 sorptometer. The power X-ray diffraction (XRD) patterns were recorded on a Bruker diffractometer using a CuKα radiation. Scanning electronic micrographs (SEM) images were obtained on LEO 1530VP. The morphology of the samples was observed by transmission electron microscopy (TEM, Hitachi-600). X-ray photoelectron spectroscopy spectra were recorded with a PerkinElmer PHI-5300 spectrometer.

$H_2$-TPR was carried out with a mixture of 5% $H_2/N_2$ as the reductive gas. The sample (0.025 g) was reduced in a flow of $H_2/N_2$ at a rate of 10 K/min. The effluent gas was monitored by TCD after removal of the product water using 5 Å molecular sieves.

### 2.3. Catalyst test

CO hydrogenation was carried out at 2.0 MPa, 1000 $h^{-1}$ and a $H_2/CO$ ration of 2.0 in a stainless-steel fixed-bed reactor with i.d. 12 mm with a catalyst loading of 2 ml. The catalyst was reduced in a flow of hydrogen at 600 K for 6 h and then cool down to ambient before switching to syngas. Liquid products and wax were collected in a cold trap and hot trap, respectively and then were offline analyzed on a GC-920 gas chromatograph that was equipped with a 35 m OV-101 capillary column.

## 3. Results

### 3.1. Catalyst texture

Similar shapes of wide-angle XRD patterns for catalysts are shown in Fig. 1. Diffraction peaks at $2\theta$ of 31.3°, 36.9°, 45.1°, 59.4° and 65.4° indicate that after calcination, cobalt was present in the form of $Co_3O_4$ crystalline phase [21,22] on all the catalysts. The mean $Co_3O_4$ crystallite sizes (Table 1) were calculated from the widths of XRD peaks using the Scherrer equation ($2\theta = 36.9°$) [1,22]. Larger $Co_3O_4$ crystallites were detected in the catalysts with higher cobalt content. An increase in cobalt loading results in sintering of cobalt oxide particles. The size of $Co_3O_4$ crystallites increases from 9.5 nm in T10 to 14.2 nm in T20 and 23.5 nm in T30.

Fig. 2 shows the low-angle XRD patterns of HMSS and catalysts. HMSS, T10 and T20 exhibit a broad diffraction peak at $2\theta = 2°$. For catalyst T10 and T20, the diffraction intensity was lower than HMSS. For catalyst T30, the diffraction peak almost disappeared. It is attributed to the partially collapse of HMSS framework during the impregnation and calcination. Fig. 3 displays the $N_2$ adsorption–desorption isotherms and pore size-distributions of the samples. It can be clearly observed that the isotherms of all samples were of classical type IV [23], which confirmed the mesoporous characteristics of HMSS and catalysts. HMSS exhibit a bimodal pore distribution with one maximum between 20 and 60 nm, and the other at ca. 2.7 nm. For catalyst after Co-loading, the range of pore

**Table 1**
Textural properties of samples.

| Samples | Pore volume ($cm^3\ g^{-1}$) | $S_{BET}$ ($m^2\ g^{-1}$) | Average pore diameter (nm) | $Co_3O_4$ Crystallite size (nm) | |
|---|---|---|---|---|---|
| | | | | XRD | TEM |
| HMSS | 2.01 | 627 | 13.4 | – | – |
| T10 | 1.28 | 499 | 9.9 | 9.5 | 8.0 |
| T20 | 1.03 | 413 | 9.3 | 14.2 | 11.3 |
| T30 | 0.75 | 321 | 9.1 | 23.5 | 20.0 |

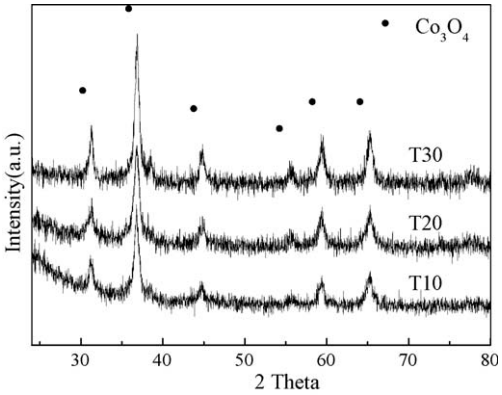


**Fig. 1.** Wide-angle XRD patterns of catalysts.

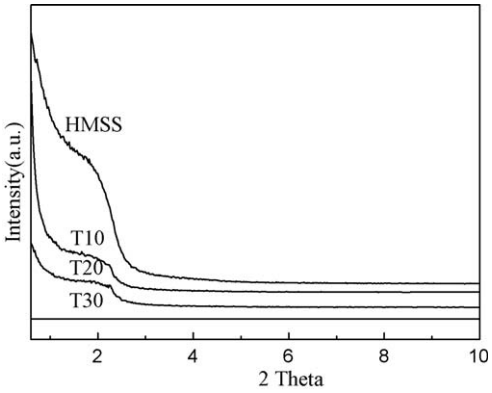


**Fig. 2.** Low-angle XRD patterns of HMSS and catalysts.

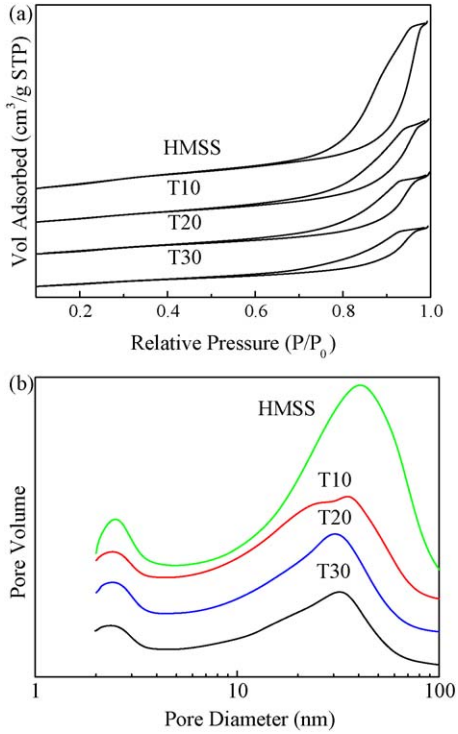


**Fig. 3.** $N_2$ adsorption/desorption isotherms (a) and BJH pore size distribution (b) of HMSS and catalysts.

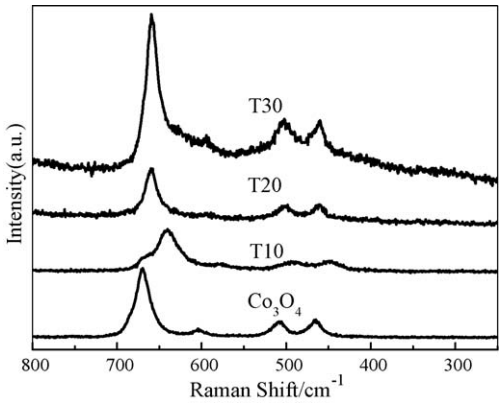


**Fig. 4.** Raman spectra of catalysts.

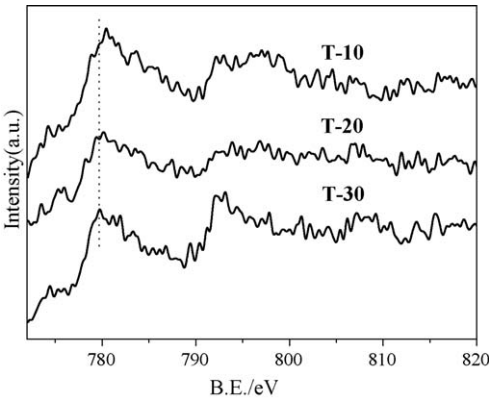


**Fig. 5.** $Co_{2p}$ XPS spectra of cobalt catalysts.

size distribution narrowed. At the same time, the mean mesopore size decreased from 40 nm (HMSS) to ca. 30 nm. From all the above results, it can be concluded that $Co_3O_4$ nano-particles were loaded in the pores of HMSS by using "two-solvent" technique [19]. Therefore, the diffraction intensity peak decreased at low-angle and even disappeared and the pore size distribution narrowed.

Table 1 displays the textural properties of the primary HMSS and catalysts. After loaded with cobalt, the BET surface area was significantly reduced. In the same way, the total pore volume was also reduced. This effect was especially pronounced for the catalysts with higher cobalt loadings [21]. Since it has been shown that the BET surface and pore volume of the catalysts lower remarkably by cobalt loading, it is reasonable to see that most of Co particles can be held inside the pores. The presences of plugging also result in narrowing the average pore diameter for catalysts. All of the data suggested that considerable amount of cobalt were present inside the pore system of HMSS [21]. The results obtained for the catalyst showed that the porous structure of HMSS was not completely destroyed and was still present even in catalyst with higher cobalt loading.

### 3.2. Dispersibility of supported cobalt oxide

Raman spectroscopy allows identification of cobalt oxidized species in cobalt catalysts. General $Co_3O_4$ displays in the Raman spectra a strong peak at 684 cm$^{-1}$ and two weak peaks at 513 and 477 cm$^{-1}$ [1]. For the catalysts, all characteristic peaks shift toward lower frequencies after cobalt loading because the HMSS were supported by highly small cobalt nano-particles [24], as shown in Fig. 4. This shift was significant for low cobalt loading. It is suggested that higher dispersion and smaller $Co_3O_4$ nano-particles were presented in lower cobalt content.

The results of XPS experiments are presented in Fig. 5. $Co_{2p}$ XPS spectra show that $Co_3O_4$ is the dominant cobalt phase in oxidized

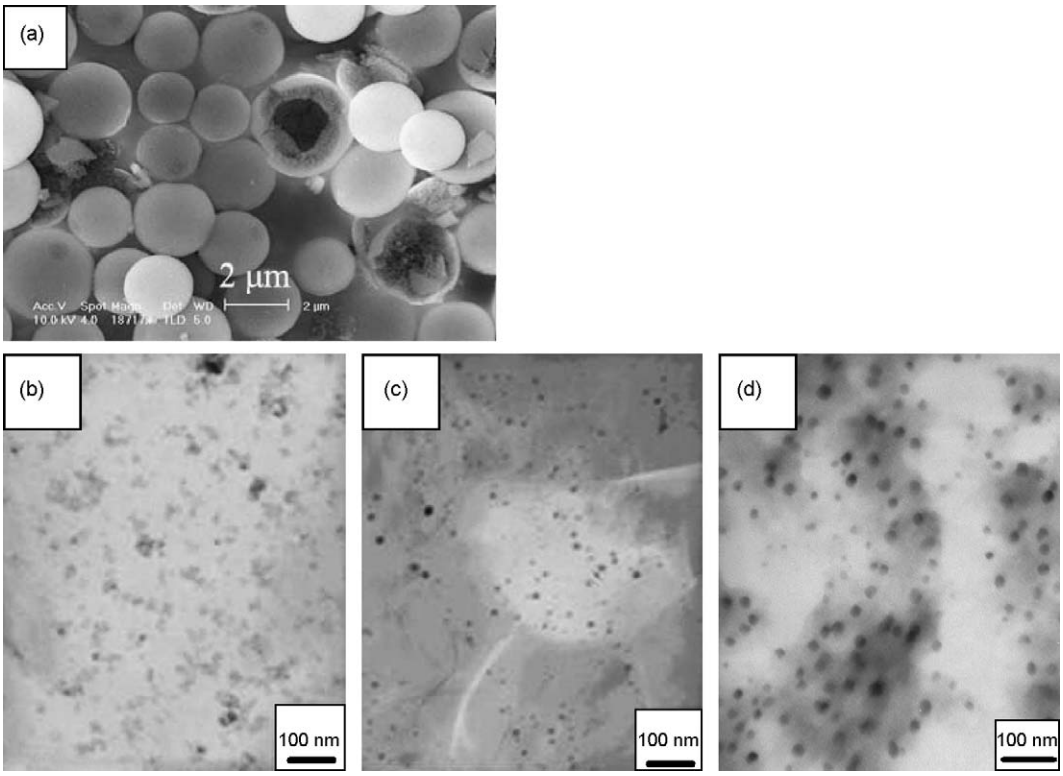


**Fig. 6.** SEM images of HMSS (a) and TEM images of catalyst T10 (b), T20 (c) and T30 (d) after silica removed with NaOH.

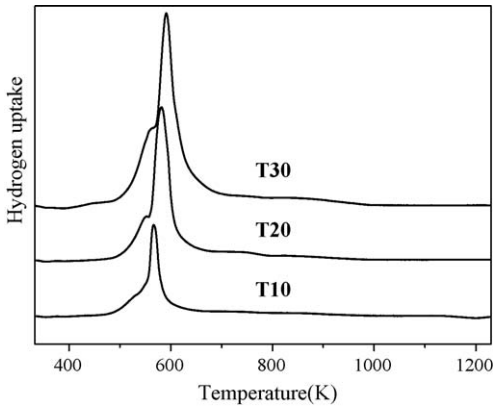


**Fig. 7.** $H_2$-TPR of cobalt catalyst.

catalysts. This finding consistent with the observation of $Co_3O_4$ patterns in all catalysts. A shift of the XPS lines toward the higher energy region in the low cobalt-loaded sample could be related to a high dispersion of the cobalt oxide phase, which determines a high proportion of cobalt in the small $Co_3O_4$ particles to be intimate contact with the HMSS support [1,21].

Fig. 6a shows the SEM image of HMSS. The morphology of HMSS was of spheres with a diameter about 1–3 μm. The broken one shows the hollow structure of HMSS and the shell ca. 500 nm. Because of the thick shell, it is difficult to characterize the cobalt particles loaded in the interior void of HMSS. Therefore, the silica host was removed with NaOH (suspending 1 g of catalyst powder in 100 ml of 2 mol $L^{-1}$ solution at room temperature for 4 h) to reveal the size of the cobalt particles. Fig. 6b, c and d shows the TEM images of catalysts after silica being eroded. It is obvious that the size of $Co_3O_4$ increased with the increasing loaded cobalt content. Significant differences in crystallite size obtained by TEM for three catalysts are shown in Table 1. In agreement with reference [13], some discrepancies have been found between crystallite particles sizes of $Co_3O_4$ particles measured using XRD and TEM. This result could be attributed to the Scherrer equation overestimate the size of crystallite particles calculated from the width of XRD patterns [1].

From above-mentioned observations, it could be concluded that nano-particles $Co_3O_4$ are highly dispersed in the channels and interior void space of HMSS. Because of more supported cobalt species in the pores of HMSS results in sintering of cobalt oxide particles. The crystallite size increases with the loaded cobalt content.

### 3.3. Reduction of supported cobalt oxide

The $H_2$-TPR profiles for the catalysts are shown in Fig. 7. The three catalysts have similar reduction profiles with two main reduction peaks, which are close to each other temperature less than 673 K. The first peak could be assigned to the reduction of $Co_3O_4$ to CoO, and the second peak corresponds to the subsequent reduction of CoO to $Co^0$ [1,21,25]. The third small reduction feature at 673–923 K as the may reflect the reduction of cobalt silicates. Khodakov et al. [26] suggested that the interaction between small particles and support was stronger than large particles and this interaction was likely to stabilize small oxidized particles and clusters in silica. From the crystallite size obtained by TEM, the sequence of particles size is T10 < T20 < T30. This particles distribution might explain the different $H_2$ reducing behaviour, as shown in Fig. 7. Interactions between smaller cobalt particles and SiOH groups in HMSS support may retard reduction. The reducibilities of the catalysts are T10 < T20 < T30.

### 3.4. Catalytic activity in F–T synthesis

The results of syngas conversion and product distribution over cobalt catalysts supported on the HMSS are listed in Table 2. It is clear that CO conversion and $C_{5+}$ selectivity increased with increasing loaded cobalt content. Catalyst T10 with the smallest crystallite size of 8.0 nm presents the lowest CO conversion and the highest methane selectivity. Small cobalt particles in T10 could be easily reoxidized by water and $CO_2$, and thus become inactive under F–T synthesis [2]. It is known that larger $Co_3O_4$ particles are active for F–T synthesis [26]. As seen in Table 2, both T20 and T30 present higher $C_{5+}$ selectivity than T10. It is consider that the presence of larger cobalt particles leads to higher selectivity to heavier hydrocarbons [3]. This observation suggests that the extent of crystallization of cobalt species is related closely to the catalytic performance. We have shown that the crystallization and reduction of T30 proceeds to a larger extent than T20 and T10, and former exhibits higher F–T activity. These results point that the high degree of cobalt crystallization means weak interaction with HMSS support and thus leads to the ready reduction to metallic cobalt, which catalyzes F–T synthesis effectively.

For the reference of MCM-41(30), the CO conversion is lower than that of T30, the selectivity of $CH_4$ was higher than that of T30, and the selectivity of $C_5$–$C_{18}$ was lower than that of T30. In general, HMSS support cobalt catalysts, which possesses a bimodal pore structure, shows better activity and $C_5$–$C_{18}$ selectivity. The catalytic feature of the three catalysts is that $C_5$–$C_{18}$ hydrocarbons are the main hydrocarbon products, which might be related to the unique structure of the support. HMSS with bimodal pore distribution facilitates reactants to access the active sites and to transport higher hydrocarbon products.

**Table 2**
Catalytic performance of catalysts for F–T synthesis.

| Catalysts | Reaction temperature (K) | CO conversion (%) | Hydrocarbon selectivity (wt.%) | | | | | |
|---|---|---|---|---|---|---|---|---|
| | | | $C_1$ | $C_2$–$C_4$ | $C_5$–$C_{11}$ | $C_{12}$–$C_{18}$ | $C_{5+}$ | $C_{19+}$ |
| T10 | 493 | 25.4 | 27.9 | 7.6 | 14.4 | 33.6 | 64.5 | 16.1 |
| | 503 | 48.2 | 23.9 | 4.4 | 22.3 | 38.4 | 71.7 | 11.0 |
| T20 | 493 | 50.0 | 12.6 | 2.9 | 28.0 | 30.4 | 82.6 | 26.2 |
| | 503 | 64.1 | 13.9 | 3.5 | 25.2 | 31.9 | 84.6 | 25.6 |
| T30 | 493 | 84.1 | 4.9 | 1.6 | 26.2 | 26.9 | 93.6 | 40.5 |
| | 503 | 84.9 | 7.1 | 2.2 | 26.8 | 30.2 | 90.7 | 33.8 |
| MCM-41(30) | 493 | 70.3 | 12.3 | 2.9 | 18.5 | 22.7 | 84.8 | 43.6 |
| | 503 | 73.6 | 13.9 | 3.2 | 19.8 | 23.1 | 82.9 | 40.0 |

Reaction conditions: $n(H_2)/n(CO) = 2.0$, GHSV = 1000 $h^{-1}$, $P$ = 2.0 MPa.

## 4. Conclusion

In summary, $Co_3O_4$ nano-particles have been successfully loaded in HMSS by two-solvent technique. The cobalt catalysts supported on HMSS are highly dispersed. The F–T catalytic behavior of cobalt species can be affected by Co loading. Lower F–T activity and higher methane selectivity observed on low cobalt loading catalyst are principally attributed to the small cobalt particles could be easily reoxidized by water and other reaction products. With increasing Co loading, the cobalt crystallite size increases and leads to good catalytic performance and high $C_{5+}$ selectivity. In this work, it is proposed that the unique bimodal pore distribution and hollow structure facilitates reactants to access the active sites. Therefore, the number of active sites available for CO adsorption increases, leading to higher catalytic activity for F–T synthesis.

## Acknowledgement

The financial support from the National Basic Research Program of China (No. 2005CB221402) was acknowledged.

## References

[1] A.Y. Khodakov, W. Chu, P. Fongarland, Chem. Rev. 107 (2007) 1692.
[2] E. Iglesia, Appl. Catal. A-Gen. 161 (1997) 59.
[3] H.L. Li, J.L. Li, H.K. Ni, D.C. Song, Catal. Lett. 110 (2006) 71.
[4] J. El Haskouri, S. Cabrera, C.J. Gomez-Garcia, C. Guillem, J. Latorre, A. Beltran, D. Beltran, M.D. Marcos, P. Amoros, Chem. Mater. 16 (2004) 2805.
[5] H.L. Li, S.G. Wang, F.X. Ling, J.L. Li, J. Mol. Catal. A-Chem. 244 (2006) 33.
[6] A.Y. Khodakov, A. Griboval-Constant, R. Bechara, F. Villain, J. Phys. Chem. B 105 (2001) 9805.
[7] F. Rohr, O.A. Lindvag, A. Holmen, E.A. Blekkan, Catal. Today 58 (2000) 247.
[8] A. Kogelbauer, J.G. Goodwin, R. Oukaci, J. Catal. 160 (1996) 125.
[9] J.L. Li, N.J. Coville, Appl. Catal. A-Gen. 181 (1999) 201.
[10] K. Jothimurugesan, S.K. Gangwal, Ind. Eng. Chem. Res. 37 (1998) 1181.
[11] S. Bessell, Appl. Catal. A-Gen. 126 (1995) 235.
[12] Z.W. Liu, X.H. Li, K. Asami, K. Fujimoto, Energ. Fuel 19 (2005) 1790.
[13] A.Y. Khodakov, A. Griboval-Constant, R. Bechara, V.L. Zholobenko, J. Catal. 206 (2002) 230.
[14] Øyvind Borg, P.D.C. Dietzel, A.I. Spjelkavik, J. Catal. 259 (2008) 161.
[15] J. Panpranot, J.G. Goodwin, A. Sayari, J. Catal. 211 (2002) 530.
[16] Y. Ohtsuka, Y. Takahashi, M. Noguchi, T. Arai, S. Takasaki, N. Tsubouchi, Y. Wang, Catal. Today 89 (2004) 419.
[17] D.H. Yin, W.H. Li, W.S. Yang, H.W. Xiang, Y.H. Sun, B. Zhong, S.Y. Peng, Micropor. Mesopor. Mater. 47 (2001) 15.
[18] M. Arruebo, M. Galan, N. Navascues, C. Tellez, C. Marquina, M.R. Ibarra, J. Santamaria, Chem. Mater. 18 (2006) 1911.
[19] I. Lopes, N. Hassan, H. Guerba, G. Wallez, A. Davidson, Chem. Mater. 18 (2006) 5826.
[20] G. Schulz-Ekloff, J. Rathousky, A. Zukal, Int. J. Inorg. Mater. 1 (1999) 97.
[21] A.Y. Khodakov, R. Bechara, A. Griboval-Constant, Appl. Catal. A-Gen. 254 (2003) 273.
[22] E. Lira, C.M. López, F. Oropeza, J. Mol. Catal. A: Chem. 281 (2008) 146.
[23] K.S.W. Sing, D.H. Everett, R.A.W. Haul, L. Moscou, R.A. Pierotti, J. Rouquerol, T. Siemieniewska, Pure Appl. Chem. 57 (1985) 603.
[24] I. Lopes, N. El Hassan, H. Guerba, G. Wallez, A. Davidson, Chem. Mater. 18 (2006) 5826.
[25] M. Ojeda, F.J. Perez-Alonso, P. Terreros, S. Rojas, T. Herranz, M.L. Granados, J.L.G. Fierro, Langmuir 22 (2006) 3131.
[26] A.Y. Khodakov, J. Lynch, D. Bazin, B. Rebours, N. Zanier, B. Moisson, P. Chaumette, J. Catal. 168 (1997) 16.